Contrib Mineral Petrol (2007) 154:647–661
DOI 10.1007/s00410-007-0214-8

ORIGINAL PAPER

A modified iterative sandwich method for determination of near-solidus partial melt compositions. II. Application to determination of near-solidus melt compositions of carbonated peridotite

Rajdeep Dasgupta · Marc M. Hirschmann

Received: 13 November 2006 / Accepted: 3 May 2007 / Published online: 1 June 2007

Abstract We performed modified iterative sandwich experiments (MISE) to determine the composition of carbonatitic melt generated near the solidus of natural, fertile peridotite + CO_2 at 1,200–1,245°C and 6.6 GPa. Six iterations were performed with natural peridotite (MixKLB-1: Mg# = 89.7) and ~10 wt% added carbonate to achieve the equilibrium carbonatite composition. Compositions of melts and coexisting minerals converged to a constant composition after the fourth iteration, with the silicate mineral compositions matching those expected at the solidus of carbonated peridotite at 6.6 GPa and 1,230°C, as determined from a sub-solidus experiment with MixKLB-1 peridotite. Partial melts expected from a carbonated lherzolite at a melt fraction of 0.01–0.05% at 6.6 GPa have the composition of sodic iron-bearing dolomitic carbonatite, with molar Ca/(Ca + Mg) of 0.413 ± 0.001, Ca# [100 × molar Ca/(Ca + Mg + Fe*)] of 37.1 ± 0.1, and Mg# of 83.7 ± 0.6. SiO_2, TiO_2 and Al_2O_3 concentrations are 4.1 ± 0.1, 1.0 ± 0.1, and 0.30 ± 0.02 wt%, whereas the Na_2O concentration is 4.0 ± 0.2 wt%. Comparison of our results with other iterative sandwich experiments at lower pressures indicate that near-solidus carbonatite derived from mantle lherzolite become less calcic with increasing pressure. Thus carbonatitic melt percolating through the deep mantle must dissolve cpx from surrounding peridotite and precipitate opx. Significant FeO* and Na_2O concentrations in near solidus carbonatitic partial melt likely account for the ~150°C lower solidus temperature of natural carbonated peridotite compared to the solidus of synthetic peridotite in the system CMAS + CO_2. The experiments demonstrate that the MISE method can determine the composition of partial melts at very low melt fraction after a small number of iterations.

Keywords Carbonatite · Experimental petrology · Iterative sandwich experiments · Mantle peridotite · Partial melting

Communicated by T.L. Grove.

R. Dasgupta · M. M. Hirschmann
Department of Geology and Geophysics,
University of Minnesota, 310 Pillsbury Drive SE,
Minneapolis, MN 55455, USA

R. Dasgupta (✉)
Lamont-Doherty Earth Observatory,
Columbia University, 61 Route 9W,
Palisades, NY 10964, USA
e-mail: rajdeep@ldeo.columbia.edu

Introduction

The upper mantle contains traces of carbon, with estimates ranging from 50–200 ppm CO_2 in typical upper mantle sampled by ridges (Marty and Tolstikhin 1998; Saal et al. 2002) up to 4,000 ppm in domains of mantle sampled by enriched mid-ocean ridge basalts and plumes (Pineau et al. 2004). If present as carbonate, these trace quantities of carbon have significant influence on partial melting processes in the upper mantle (Wyllie and Huang 1975; Eggler 1976) and carbonatite may be the deepest melt formed by incipient fusion of peridotite in upwelling mantle (Dasgupta and Hirschmann 2006). The partial melts generated at great depth from peridotite with 50–200 ppm carbon likely affect the geophysical properties of the deep upper mantle as well as Earth's geochemical evolution (Dasgupta and Hirschmann 2006), but there are few direct constraints on their composition.

Experimental determination of the compositions of carbonatitic partial melts generated at the solidus of carbonated peridotite is challenging, as near-solidus partial melting experiments with small concentrations of CO_2 produce very small melt pools, commonly less than a micron in diameter, and because the quenched melts produce a texturally inhomogeneous aggregate of phases (Dasgupta and Hirschmann 2006). Experiments aimed at obtaining reliable compositions of quenched carbonate partial melts of peridotite employ ≥4 wt% bulk CO_2 (Wallace and Green 1988; Sweeney 1994; Dalton and Presnall 1998; Gudfinnsson and Presnall 2005). However, natural mantle rocks have a high thermodynamic variance and consequently a high added proportion of carbonate unavoidably affects the compositions of coexisting minerals and melts (Dasgupta et al. 2005; Dasgupta and Hirschmann 2007), unless the added carbonate fortuitously has the composition of the equilibrium melt. For example, large amounts of added carbonate can alter the Ca/(Ca + Mg) of the bulk rock and thereby influence the Ca/(Ca + Mg) of near-solidus partial melts (Dasgupta et al. 2005). Also, excess CO_2 increases the fraction of carbonatite melt produced near the solidus, thereby diluting the incompatible elements such as alkalis in the resulting melt (Dasgupta et al. 2005; Dasgupta and Hirschmann 2007).

To determine accurately the composition of very small degree partial melts, Hirschmann and Dasgupta (2007) developed the modified iterative sandwich experiment (MISE) technique. In this method, the composition of a near-solidus partial melt of a target lithology is determined iteratively from experiments in which the target lithology is equilibrated with a small amount of added material with the composition similar to the near-solidus partial melt. In successive iterations, the composition of the added material is ascertained from bulk rock/melt partition coefficients determined in the preceding experimental step. It can be shown that this approach will produce partial melts characteristic of incipient partial melting of the target lithology after a modest number of iterations (Hirschmann and Dasgupta 2007). Here, we apply the MISE technique to determine the composition of incipient partial melt of carbonated fertile peridotite at 6.6 GPa. First generation of incipient carbonatitic partial melts from upwelling mantle beneath oceanic ridges may occur at a pressure of 300 km (Dasgupta and Hirschmann 2006), so detailed compositional information of primary carbonatite derived from natural peridotite is most desirable at a pressure of 10 GPa. But application of MISE to determine near-solidus melt compositions benefits from prior knowledge of the solidus temperature of the target lithology at a given pressure. As the solidus of carbonated peridotite with trace carbon content is best constrained at a pressure of 6.6 GPa (Dasgupta and Hirschmann 2007), we chose the same nominal pressure for carrying out the present experiments.

Experimental procedures

Methodology

We sought to determine the near-solidus partial melt composition of a carbonated peridotite with total carbon comparable to the small quantities thought to prevail in the convecting upper mantle (50–200 ppm: Marty and Tolstikhin 1998; Saal et al. 2002) at 6.6 GPa. At this pressure, a peridotite with small amounts of CO_2 will also have a small fraction of magnesite at the solidus. However, performing experiments with coexisting magnesite and carbonatite would present a challenge for the MISE method, as it would be difficult to control the melt fraction from one iteration to another. Instead we aimed to characterize the composition of partial melt that would be in equilibrium with silicate residua just after the exhaustion of magnesite. For mantle with 50–200 ppm CO_2, this would occur at 0.01–0.05% melting (i.e., $F = 1–5 \times 10^{-4}$). Following the methodology of Hirschmann and Dasgupta (2007), we performed iterative sandwich experiments in which the same nominally carbonate-free fertile peridotite composition (the ''bread'') was repeatedly equilibrated with an added portion of carbonate (the ''meat''), which was adjusted at each iteration according to the results of the preceding experiment.

The composition of the ''meat'' for the initial iteration was an approximate estimate of the near-solidus partial melt bulk composition based on the results of the previous experiments in CMAS + CO_2 systems at similar pressures (Dalton and Presnall 1998) and from the experiments with natural compositions at lower pressures (Wallace and Green 1988; Thibault et al. 1992). For each subsequent iteration, the composition of the ''meat'' was determined from the bulk peridotite/melt partition coefficients, $\overline{D}_i$, for each element, i, according to the batch melting equation applicable at the solidus, $C_i^0/\overline{D}_i$, where C_i^0 is the concentrations of the ith element in the nominally carbonate-free peridotite (the ''bread'') (Hirschmann and Dasgupta 2007). Strictly speaking the relation $C_i^0/\overline{D}_i$ is appropriate for determining the partial melt composition at a melt fraction of zero ($F = 0$), but this relation also applies for the small melt fractions of interest in this study ($F \leq 5 \times 10^{-4}$), so long as $F << \overline{D}_i$, which should be true for all major and minor elements of interest. In other words, the near-solidus liquid determined by this approach is characteristic of liquids generated near the solidus in the interval where major and minor element compositions of residual silicate minerals are affected negligibly by melting. Values of $\overline{D}_i$ were determined from the mineral/melt partition coefficients determined from phase compositions from the previous iteration and the mode of minerals present near the solidus of carbonated peridotite, as determined from a

CO_2-free experiment performed at the same temperature as the iterative sandwich experiments.

Starting materials

The ''bread'' of fertile peridotite composition (MixKLB-1; Table 1) was prepared from a mixture of clean natural olivine, opx, cpx, and garnet (Dasgupta and Hirschmann 2006). Compositions of individual minerals were determined by electron microprobe analyses of 4–6 randomly selected grains for each mineral. The reported composition of silicate bread MixKLB-1 (Table 1) is based on a mass balance calculation using weighed proportions of each phase and their respective compositions. Minerals were thoroughly mixed and ground to <5 μm grain size in an agate mortar under ethanol. The rock powder was dehydrated by firing at 1,000°C for 4 h in a one-atmosphere furnace at an oxygen partial pressure approximately one order of magnitude below the quartz-magnetite-fayalite buffer (QFM-1), fixed by a mixture of CO and CO_2 gases. The mix was then reground under ethanol and stored in a drying oven at 120°C. The composition of the added carbonate ''meat'' at each iteration was constructed by mixing a combination of natural magnesite ($MgCO_3$), siderite ($FeCO_3$) and reagent grade carbonates ($CaCO_3$, Na_2CO_3, and K_2CO_3), oxides (SiO_2, TiO_2, Al_2O_3, and FeO), and silicate (Mg_2SiO_4) (Table 1). These were dried at one atmosphere ($CaCO_3$ and $MgCO_3$ at 300°C for 7–20 h, Na_2CO_3 at 250°C for 4 h, SiO_2 at 1,100°C for 30 h, TiO_2 at 1,000°C for 16 h, Al_2O_3 at 1,200°C for 18 h) and stored in a desiccator before weighing. Reported compositions of constructed melts for each iteration (Table 1) are based on weighed proportions of various compounds.

Experimental and analytical procedures

All experiments were performed in a 1,000-ton Walker-style multi-anvil apparatus at 6.6 GPa following the assembly and calibration described in Dasgupta et al. (2004). Temperature was controlled with a $W_{97}Re/W_{75}Re$ thermocouple next to the capsule and oriented axially with respect to the heater. Pressure and temperature uncertainties are believed to be ±0.3 GPa, ±10°C. Nominal temperatures of the experiments were chosen based on the location of the natural peridotite + CO_2 solidi as determined by Dasgupta and Hirschmann (2006, 2007) at 6.6 GPa. Target temperatures for the final iterations (4 through 6) were chosen to ensure absence of residual magnesite, i.e., 10–20°C higher than the expected solidus locations based on the trend of bulk Na_2O/CO_2 ratio versus solidus temperatures at 6.6 GPa (Dasgupta and Hirschmann 2007). Short run times (≤48 h) were preferred to minimize the influx of hydrogen from the assembly into the capsule (Dalton and Wood 1993). Capsules were formed from high purity Au tubing with 2 mm outer and

Table 1 Compositions of starting mixes

	Starting minerals in the bread					Bread	Meat				
	ol	opx	cpx	cpx	gt	MixKLB-1	Melt#1	Melt#2	Melt#3	Melt#4	Melt#5
SiO_2	40.80	57.43	48.60	54.74	41.32	44.54	5.06	8.87	3.75	3.85	4.08
TiO_2	0.00	0.01	1.54	0.16	0.07	0.21	–	0.86	0.50	0.81	1.16
Al_2O_3	0.02	0.77	9.37	9.60	22.69	3.70	–	–	–	0.40	0.34
Cr_2O_3	0.02	0.37	0.01	0.09	1.75	0.23	–	–	–	–	–
FeO*	8.93	4.03	7.16	2.95	11.76	8.08	2.96	4.77	5.39	5.75	7.68
MnO	0.12	0.10	0.14	0.03	0.39	0.14	–	–	–	–	–
MgO	50.12	36.82	13.81	11.21	17.08	39.30	18.79	17.19	18.77	17.05	22.19
CaO	0.07	0.30	18.39	16.94	5.05	3.52	25.55	16.98	22.42	24.26	21.19
Na_2O	0.00	0.06	0.99	4.11	0.02	0.29	2.73	9.55	4.56	3.94	4.22
K_2O	0.00	0.01	0.02	0.02	0.01	0.01	0.20	–	–	–	–
CO_2	–	–	–	–	–	–	44.42	41.80	44.64	43.98	39.17
Mg#	90.91	94.21	77.28	87.11	72.13	89.65	91.88	86.52	86.13	84.08	83.73
Ca#		0.01	0.43	0.49	0.13	0.05	0.47	0.38	0.43	0.46	0.36
Added minerals	–	–	–	–	–	ol, opx, cpx, gt	cc, mst, sid, nc,kc, qtz	cc, mst, sid, nc, TiO_2, qtz	cc, mst, sid, nc TiO_2, Al_2O_3, qtz	cc, mst, sid, nc TiO_2, Al_2O_3, qtz	cc, mst, sid, nc FeO, TiO_2, Al_2O_3, fo

FeO*, Total Fe; Mg#, 100 × molar MgO/(MgO + FeO*); Ca#, molar CaO/(CaO + MgO + FeO*). The compositions of the minerals in the starting mixes are re-reported from the supplementary information of Dasgupta and Hirschmann (2006)

ol olivine, *opx* orthopyroxene, *cpx* clinopyroxene, *gt* garnet, *cc* calcite, *mst* magnesite, *sid* siderite, *nc* sodium carbonate, *kc* potassium carbonate, *qtz* quartz, *fo* forsterite

1.8 mm inner diameter. Approximately 90% by weight of peridotite (bread) and 10% by weight of carbonate mixture (meat) were loaded into the capsules with the layer of carbonate typically sandwiched between two layers of peridotite. For some runs, the layer was placed at one end of the capsule to achieve a larger melt pool at the end of the experiment. However, even in these runs the final location of large melt pools were typically towards the corners or the sides of the capsule. A total of 4 to 6 mg sample powders were loaded, and then the Au containers were placed in a drying oven at ~120°C for a couple of hours prior to welding the top shut. The sealed capsules were compressed into 2.2–2.8 mm compact cylinders in a steel die. The entire octahedral assemblies were dried at 120°C in a vacuum oven before running the experiments.

Because quenched carbonate melts are delicate and water-soluble, the samples were polished without water. After the first iteration, the capsule was cut in half longitudinally into two halves using a wire-saw and then polished to a 1/4 μm finish using diamond powder. However, the lubricant oil of the wire saw damaged the fragile melt pools, and so the saw was avoided in subsequent iterations. Instead, run products were ground longitudinally on a strip grinder and then polished on soft nylon cloth using dry polycrystalline diamond powders. No water or oil was used during either the grinding or polishing. Repeated vacuum impregnation with low viscosity epoxy resin (PETROPOXY 154) was necessary to minimize polishing damage of the quenched melt regions.

Quantitative and textural analyses of run products were performed using a JEOL JXA8900R electron microprobe (Table 3). Accelerating voltage of 15 kV and a ZAF matrix correction routine were used for WDS quantitative analyses. Counting times for peak and for backgrounds were 20 and 10 s, respectively for silicates and 10 and 5 s for carbonates. For silicate minerals, a focused 20 nA beam was used, but for carbonate minerals and quenched melts we employed a defocused beam of 2–5 μm and 5–20 μm diameter, respectively and a current of 1–8 nA, depending on the grain size or the dimension of the interstitial quenched melt pool. Natural olivine, orthopyroxene, clinopyroxene, garnet, hornblende, dolomite, siderite, chromite, feldspar, and a basalt glass were used as analytical standards. To ensure accuracy and precision of analytical data, olivine, opx, cpx, garnet, dolomite, and basalt glass of known compositions were analyzed in each probe session as secondary standards.

Results

Summaries of run conditions, resulting phase assemblages, and calculated phase proportions are given in Table 2 and compositions of quenched melt and residual minerals are detailed in Tables 3, 4, 5, 6, 7, 8 and plotted as a function of iteration number in Figs. 2, 3, 4, 5.

Phase assemblage and textures

At 6.6 GPa and 1230 °C, unadulterated MixKLB-1 produces a homogeneous subsolidus mineral assemblage consisting of olivine (63 wt%), opx (9 wt%), cpx (15 wt%), and garnet (13 wt%) (Table 2). Runs with an added layer of carbonate-rich ''meat'' produce all of these phases together with a layer of magnesite solid solution (≤9%; Fig. 1a) and/or quenched carbonatitic melt (≤11%). Pools of quenched melt are always found segregated in one corner or mostly to the side of the capsule (Fig. 1b), irrespective of the initial geometry of the charge, likely owing to thermal gradients in the assemblies. This migration of the melt phase from its initial position in the capsule presumably facilitates melt/matrix reaction, helping the melt to equilibrate with large fraction of the capsule. Also, it reduces quench modification and facilitates microbeam analysis of the quenched melt pool. Although most of the melt is located proximal to capsule walls (Fig. 1b), a small amount was observed distributed throughout the charges, either at triple grain junctions or along grain edges, of all melt-present runs (Fig. 1c). This high connectivity of carbonate-rich melt is believed to enhance equilibration of residual silicate minerals. In fact, no major element zoning was noted for olivine, opx, and cpx. However, small residual cores always remain for garnet grains and thus the average of rim compositions are reported in Table 6.

Solidus location

Nominal temperatures of the experiments performed in this study were chosen based on the solidus of natural carbonated peridotite at similar pressure (Dasgupta and Hirschmann 2006, 2007). But the solidi temperatures for the peridotite–carbonatite sandwiches were also constrained independently in this study for iterations 1 (<1,230°C), 2 (1,170–1,200°C), and 3 (1,200–1,230°C) and are in agreement with the previous studies.

Phase compositions at the 6.6 GPa solidus of natural carbonated lherzolite

In the following section we describe the compositions of six phases observed—carbonate-rich melt, cpx, garnet, opx, olivine, and magnesite.

Carbonate melt. Quenched carbonate melts are broadly magnesio-dolomitic, with molar Ca/(Ca + Mg) ranging from 0.41 to 0.49. SiO_2 concentrations vary from 4.0 to

Table 2 Summary of 6.6 GPa modifed iterative sandwich experiments (MISE)

Run#	Added melt (wt%)	T (°C)	*t* (h)	Equilibrium assemblage	Phase proportions						Σr^2	Fe loss (%)
					Ol	Opx	Cpx	Gt	Mst	CbL		
		Melt absent run (MixKLB-1)										
M180	0	1,230	48	Ol, Opx, Cpx,Gt	63.0	8.6	15.2	13.0	–	–	0.08	–
M141	0	1,325	24	Ol, Opx, Cpx, Gt	+	+	+	+	–	–		
		Iteration#1										
M158	15.2	1,225	24	Ol, Opx, Cpx, Gt, Mst, cbL	+	+	+	+	+	+		
M172	9.8	1,230	24	Ol, Opx, Cpx, Gt, Mst, cbL	51.4	5.8	19.6	13.4	3.9	6.0	0.25	5.5
M165	10.1	1,260	24	Ol, Opx, Cpx, Gt, cbL	56.3	6.0	14.3	13.6	–	9.9	0.08	1.3
M142	10.7	1,325	24	Ol, Opx, Cpx, Gt, cbL	+	+	+	+	+	+		
		Iteration#2										
M267	9.8	1,170	24	Opx, Cpx, Gt, Mst	54.8	0.0	26.9	9.8	8.5	–	0.61	5.8
M265	9.9	1,200	24	Ol, Opx, Cpx, Gt, cbL	52.0	12.3	13.8	11.4	–	10.5	0.11	3.4
		Iteration#3										
M277	9.9	1,200	24	Ol, Opx, Cpx, Gt, Mst	54.2	0.0	25.8	11.0	9.0	–	0.32	1.9
M278	9.8	1,230	24	Ol, Opx, Cpx, Gt, cbL	55.9	8.1	13.0	12.8	–	10.3	0.00	–
		Iteration#4										
M282	10.0	1,230	24	Ol, Opx, Cpx, Gt, cbL	52.8	9.6	13.6	13.0	–	11.0	0.01	0.5
M285	9.8	1,250	6	Ol, Opx, Cpx, Gt, cbL	+	+	+	+	–	+		
		Iteration#5										
M289	9.8	1,245	24	Ol, Opx, Cpx, Gt, cbL	53.3	9.9	13.0	13.9	–	10.0	0.03	1.5
		Iteration#6										
M289	9.9	1,245	24	Ol, Opx, Cpx, Gt, cbL	54.2	9.0	13.2	13.6	–	10.0	0.04	1.7

Phase proportions (wt%) are calculated by mass balance approach using measured compositions of observed phases and the bulk composition of the starting mix. – indicates absence of a phase and + indicates presence of a phase. Abbreviations are same as in Table 1; cbL, carbonatite melt. Σr^2 is the sum of squared residuals calculated using the modes of phases obtained by the mass balance calculation and illustrate a close approach to equilibrium. Fe loss is the relative percent of FeO deficit based on the estimated bulk compositions in each run and their resulting phase compositions and proportions

Table 3 Composition of carbonatite partial melt

Run#	M172	M165	M265	M278	M282	M289	M295	Average
Iteration#	1	1	2	3	4	5	6	Equilibrium
T (°C)	1,230	1,260	1,200	1,230	1,230	1,245	1,245	Composition
n	16	10	12	7	10	12	11	
SiO_2	8.9(14)	7.0(33)	4.2(26)	4.0(32)	4.1(25)	4.1 (23)	4.0 (15)	4.07 (5)
TiO_2	0.51 (22)	1.0 (3)	0.84 (56)	0.74 (39)	0.95 (37)	1.05 (17)	0.99 (23)	1.00 (5)
Al_2O_3	0.39 (2)	0.49 (13)	0.42 (25)	0.37 (27)	0.28 (17)	0.28 (17)	0.32 (20)	0.29 (2)
Cr_2O_3	ND	n.d.	0.03 (3)	0.06 (5)	0.15 (11)	0.15 (13)	0.12 (6)	0.14 (2)
FeO*	4.80 (37)	6.84 (47)	5.9 (12)	6.0 (24)	7.4 (23)	7.87 (50)	7.59 (85)	7.62 (24)
MnO	0.45 (6)	0.29 (9)	0.20 (6)	0.23 (4)	0.20 (4)	0.20 (6)	0.21 (10)	0.20 (1)
MgO	18.3 (13)	17.9 (20)	20.0 (39)	17.9 (43)	22.1 (38)	21.9 (11)	22.0 (20)	22.00 (10)
CaO	18.1 (14)	20.1 (24)	20.1 (22)	23.8 (39)	21.6 (32)	21.5 (37)	21.5 (25)	21.53 (6)
Na_2O	7.8 (20)	1.4 (11)	8.4 (34)	4.2 (22)	3.78 (65)	4.0 (12)	4.1 (13)	3.96 (16)
K_2O	0.10 (3)	0.08 (4)	0.06 (2)	0.07 (3)	0.01 (1)	0.01 (0)	0.05 (3)	0.02 (2)
CO_2	40.6 (65)	45.0 (26)	39.9 (36)	42.6 (42)	39.4 (35)	39.0 (41)	39.2 (34)	39.2 (2)
Sum	100.00	100.00	100.00	100.00	100.00	100.00	100.00	100.00
Mg#	87.18	82.31	85.82	84.29	84.13	83.22	83.78	83.71

Numbers in parentheses represent 1σ standard deviations on the basis of replicate analyses, in terms of last digit(s). For example, 8.9(14) should be read as 8.9±1.4. *n* number of analyses averaged. CO_2 is calculated by difference of 100 and the measured analytical total. ''Average equilibrium composition'' represents mean oxide concentration of iteration 4 through 6

Table 4 Composition of clinopyroxene

Run#	M180	M172	M165	M267	M265	M277	M278	M282	M289	M295	Average
Iteration#	no melt	1	1	2	2	3	3	4	5	6	'equilibrium'
T (°C)	1,230	1,230	1,260	1,170	1,200	1,200	1,230	1,230	1,245	1,245	composition
n	16	10	18	17	12	16	15	15	17	16	
SiO_2	55.42 (41)	54.54 (81)	54.67 (32)	55.30 (61)	55.37 (59)	55.77 (37)	56.09 (56)	54.87 (74)	55.23 (64)	55.13 (59)	55.08 (19)
TiO_2	0.30 (4)	0.14 (7)	0.08 (3)	0.47 (15)	0.38 (10)	0.24 (4)	0.24 (7)	0.28 (4)	0.24 (4)	0.25 (3)	0.26 (2)
Al_2O_3	2.67 (63)	2.2 (11)	1.73 (59)	4.42 (63)	4.14 (40)	2.54 (16)	2.56 (50)	2.58 (97)	2.42 (65)	2.48 (59)	2.49 (8)
Cr_2O_3	0.27 (7)	0.24 (7)	0.21 (4)	0.35 (8)	0.36 (6)	0.26 (5)	0.26 (7)	0.25 (5)	0.30 (7)	0.29 (6)	0.28 (3)
FeO*	3.75 (17)	3.57 (37)	3.25 (39)	3.75 (17)	3.82 (22)	3.77 (24)	3.79 (25)	3.53 (24)	3.88 (27)	3.78 (21)	3.73 (18)
MnO	0.14 (3)	0.10 (4)	0.09 (2)	0.12 (4)	0.11 (4)	n.d.	0.13 (4)	0.12(5)	0.11 (3)	0.11 (2)	0.11 (1)
MgO	18.72 (82)	19.61 (67)	19.48 (70)	17.05 (79)	17.91 (36)	18.41 (41)	18.52 (55)	18.53 (63)	19.45 (15)	19.32 (17)	19.10 (50)
CaO	17.28 (67)	18.7 (11)	19.2 (10)	15.52 (85)	15.65 (80)	17.29 (71)	16.88 (86)	18.3 (10)	17.58 (54)	17.68 (61)	17.85 (39)
Na_2O	1.48 (16)	1.18 (16)	1.03 (24)	2.82 (28)	2.63 (26)	1.70 (10)	1.64 (13)	1.43 (20)	1.33 (9)	1.35 (10)	1.37 (5)
K_2O	ND	0.03 (1)	0.02 (2)	0.02 (2)	0.02 (2)	0.02 (2)	0.02 (2)	0.03 (2)	0.03 (1)	0.02 (1)	0.03 (1)
Sum	100.02	100.25	99.79	99.83	100.41	100.00	100.12	99.93	100.56	100.41	100.30 (33)
Mg#	89.90	90.73	91.45	89.00	89.30	89.70	89.70	90.34	89.92	90.11	90.12 (21)

Table 5 Composition of orthopyroxene

Run#	M180	M172	M165	M267	M265	M277	M278	M282	M289	M295	Average
Iteration#	no melt	1	1	2	2	3	3	4	5	6	'Equilibrium'
T (°C)	1,230	1,230	1,260	1,170	1,200	1,200	1,230	1,230	1,245	1,245	Composition
N	13	12	11	15	9	10	8	12	9	13	
SiO_2	56.70 (52)	56.95 (22)	57.84 (25)	57.42 (17)	57.26 (41)	57.62 (30)	57.74 (36)	57.66 (34)	57.47 (30)	57.57 (30)	57.57 (10)
TiO_2	0.20 (3)	0.07 (1)	0.05 (1)	0.12 (4)	0.13 (2)	0.11 (4)	0.08 (3)	0.12 (4)	0.09 (4)	0.10 (4)	0.10 (2)
Al_2O_3	1.42 (6)	1.23 (11)	0.56 (4)	0.85 (6)	0.96 (8)	0.58 (10)	0.70 (25)	0.63 (5)	0.66 (5)	0.67 (7)	0.65 (2)
Cr_2O_3	0.12 (3)	0.12 (2)	0.05 (2)	0.07 (6)	0.11 (4)	0.04 (4)	0.09 (3)	0.08 (3)	0.06 (3)	0.07 (3)	0.07 (1)
FeO*	5.76 (13)	5.57 (13)	5.31 (6)	5.74 (8)	5.70 (13)	5.96 (3)	5.78 (14)	5.85 (8)	5.89 (18)	5.83 (18)	5.86 (3)
MnO	0.18 (2)	0.14 (1)	0.11 (1)	0.14 (3)	0.11 (3)	n.d.	0.14 (5)	0.12 (1)	0.13 (2)	0.13 (3)	0.13 (1)
MgO	34.28 (56)	35.17 (77)	35.13 (10)	35.10 (26)	34.67 (19)	34.64 (13)	34.06 (24)	34.48 (29)	34.99 (24)	34.49 (24)	34.65 (29)
CaO	1.06 (8)	1.08 (14)	0.97 (4)	0.75 (6)	0.87 (6)	0.59 (6)	0.78 (10)	0.89 (9)	0.89 (11)	0.94 (9)	0.91 (3)
Na_2O	0.22 (3)	0.14 (2)	0.12 (3)	0.25 (3)	0.26 (5)	0.13 (1)	0.19 (3)	0.15 (3)	0.16 (2)	0.17 (2)	0.16 (1)
K_2O	ND	0.03 (0)	0.02 (0)	0.02 (2)	0.02 (1)	0.01 (1)	0.01 (1)	0.02 (1)	0.03 (3)	0.02 (2)	0.02 (1)
Sum	99.93	100.50	100.16	100.47	100.09	99.67	99.57	99.99	100.38	100.00	100.12
Mg#	91.39	91.84	92.18	91.59	91.55	91.20	91.31	91.31	91.38	91.34	91.33

Table 6 Composition of garnet

Run#	M180	M172	M165	M267	M265	M277	M278	M282	M289	M295	Average
Iteration#	no melt	1	1	2	2	3	3	4	5	6	'equilibrium'
T (°C)	1230	1230	1260	1170	1200	1200	1230	1230	1245	1245	composition
n	8	9	10	9	10	9	8	8	7	8	
SiO_2	41.79 (28)	41.11 (94)	41.61 (38)	42.15 (23)	42.13 (43)	42.18 (26)	42.38 (22)	41.64 (34)	41.62 (21)	41.72 (31)	41.66 (5)
TiO_2	0.80 (10)	0.50 (12)	0.35 (14)	0.71 (4)	0.75 (8)	0.97 (6)	0.96 (7)	0.77 (34)	0.89 (4)	0.88 (5)	0.85 (7)
Al_2O_3	22.22 (51)	21.85 (63)	22.03 (42)	23.59 (33)	23.48 (25)	22.75 (29)	22.61 (27)	22.68 (32)	21.74 (32)	22.01 (41)	22.14 (48)
Cr_2O_3	0.86 (2)	0.87 (8)	1.23 (26)	0.67 (2)	0.76 (9)	0.79 (5)	0.88 (6)	0.98 (33)	0.89 (8)	0.92 (9)	0.93 (5)
FeO*	9.77 (3)	8.69 (80)	8.9 (13)	7.91 (22)	7.82 (14)	8.61 (9)	8.37 (22)	8.45 (68)	8.23 (41)	8.36 (41)	8.35 (11)
MnO	0.30 (4)	0.31 (4)	0.31 (4)	0.31 (7)	0.26 (3)	n.d.	0.28 (4)	0.33 (6)	0.24 (4)	0.26 (3)	0.28 (5)
MgO	19.23 (41)	20.8 (11)	19.5 (10)	20.81 (48)	20.69 (15)	20.40 (32)	20.59 (59)	20.42 (78)	21.07 (75)	20.98 (66)	20.82 (35)
CaO	4.91 (12)	5.40 (62)	5.64 (44)	3.79 (14)	4.05 (12)	4.29 (18)	4.63 (60)	4.59 (39)	5.14 (37)	5.04 (32)	4.92 (29)
Na_2O	0.11 (3)	0.10 (3)	0.05 (2)	0.14 (2)	0.15 (4)	0.12 (3)	0.11 (2)	0.08 (2)	0.13 (6)	0.11 (6)	0.11 (3)
K_2O	0.01 (0)	0.03 (1)	0.03 (1)	0.02 (2)	0.02 (2)	0.01 (1)	0.02 (2)	0.03 (2)	0.02 (2)	0.02 (2)	0.02 (1)
Sum	100.01	99.69	99.66	100.10	100.10	100.13	100.82	99.98	99.98	100.31	100.09
Mg#	77.82	81.03	79.60	82.43	82.51	80.85	81.42	81.15	82.03	81.73	81.64

Table 7 Composition of olivine

Run#	M180	M172	M165	M267	M265	M277	M278	M282	M289	M295	Average
Iteration#	no melt	1	1	2	2	3	3	4	5	6	'Equilibrium'
T (°C)		1,230	1,260	1,170	1,200	1,200	1,230	1,230	1,245	1,245	Composition
n	12	11	13	14	11	16	10	12	16	17	
SiO_2	40.76 (26)	40.23 (35)	41.04 (24)	40.82 (55)	40.58 (19)	40.20 (64)	40.72 (16)	40.91 (17)	40.48 (15)	40.69 (15)	40.69 (22)
TiO_2	0.04 (3)	0.02 (2)	0.02 (2)	0.04 (2)	0.04 (3)	0.05 (7)	0.02 (2)	0.03 (2)	0.03 (4)	0.03 (2)	0.03 (0)
Al_2O_3	0.14 (11)	0.04 (9)	0.19 (15)	0.04 (8)	0.05 (10)	0.14 (7)	0.02 (2)	0.05 (7)	0.05 (5)	0.05 (3)	0.05 (0)
Cr_2O_3	0.05 (4)	0.01 (2)	0.02 (4)	0.02 (2)	0.02 (3)	0.03 (6)	0.01 (2)	0.03 (3)	0.02 (2)	0.02 (2)	0.02 (1)
FeO*	9.45 (8)	8.71 (23)	8.54 (18)	9.24 (23)	9.14 (16)	9.70 (9)	9.32 (13)	9.18 (16)	9.21 (7)	9.19 (7)	9.19 (2)
MnO	0.11 (3)	0.10 (3)	0.10 (4)	0.13 (3)	0.12 (4)	0.13 (6)	0.10 (5)	0.11 (3)	0.10 (2)	0.10 (2)	0.10 (1)
MgO	48.97 (45)	50.44 (40)	49.9 (12)	49.51 (57)	50.03 (36)	49.1 (12)	49.50 (21)	49.56 (32)	49.94 (19)	49.74 (29)	49.75 (19)
CaO	0.13 (12)	0.16 (10)	0.14 (10)	0.13 (11)	0.11 (4)	0.19 (22)	0.13 (4)	0.11 (4)	0.13 (4)	0.12 (3)	0.12 (1)
Na_2O	0.02 (2)	0.03 (3)	0.03 (2)	0.03 (3)	0.02 (2)	0.02 (2)	0.02 (2)	0.02 (1)	0.02 (1)	0.02 (1)	0.02 (0)
K_2O	ND	0.02 (1)	0.02 (1)	0.02 (2)	0.02 (2)	0.02 (1)	0.01 (1)	0.02 (2)	0.02 (2)	0.02 (1)	0.02 (0)
Sum	99.67	99.79	99.98	99.97	100.13	99.56	99.85	100.01	100.00	99.98	100.00
Mg#	90.23	91.17	91.24	90.52	90.71	90.01	90.44	90.58	90.62	90.61	90.60

Table 8 Composition of magnesite

Run#	M172	M267	M277
Iteration#	1	2	3
T (°C)	1,230	1,170	1,200
n	10	15	12
SiO_2	0.00	0.03 (3)	0.03 (4)
TiO_2	0.01 (2)	0.01 (1)	0.01 (2)
Al_2O_3	0.02 (2)	0.01 (3)	0.01 (1)
Cr_2O_3	ND	0.02 (2)	0.01 (2)
FeO*	5.40 (37)	5.36 (12)	5.41 (26)
MnO	0.07 (19)	0.13 (4)	0.11 (4)
MgO	43.64 (62)	41.76 (34)	41.30 (32)
CaO	2.07 (29)	1.85 (21)	1.40 (16)
Na_2O	0.05 (6)	0.02 (2)	0.01 (1)
K_2O	0.01 (2)	0.03 (2)	0.02 (2)
CO_2	48.73 (91)	50.91 (31)	51.68 (34)
Sum	100.00	100.12	100.00
Mg#	93.50	93.29	93.16

CO_2 is calculated by stoichiometry

8.9%, though concentrations in iterations 2 onward are in the narrow interval of 4.0–4.2 wt%. TiO_2 concentrations range from 0.5 to 1.1 wt% and Al_2O_3 concentrations range from 0.3 to 0.5 wt%. FeO* concentrations range from 4.8 to 7.9% and Mg#s from 82.3 to 87.2. Na_2O ranges dramatically from 1.4 to 8.4 wt%, but the variation is chiefly in the first 3 iterations; the range in the final three iterations is from 3.8 to 4.1 wt%. Concentrations of CO_2 derived from microprobe totals range from 45 to 39 wt%. Although the experiments were nominally anhydrous, some contamination with H_2O is surely unavoidable. Thus, the melts likely had some small uncharacterized concentration of H_2O and the actual CO_2 concentration of the melts may be slightly less than that inferred from microprobe totals.

Clinopyroxene. Clinopyroxene is magnesian and diopside-rich, with CaO ranging from 15.5 to 19.2 wt% and with Mg#s from 89.3 to 91.5 (Table 4). Al_2O_3 contents range from 1.7 to 4.4 wt%, and Na_2O concentrations vary between 1.03 and 2.8 wt%.

Orthopyroxene. Orthopyroxene has Mg#s from 91.2 to 92.2 and from 0.6 to 1.1 wt% CaO. Al_2O_3 contents range from 0.6 to 1.4 wt%.

Garnet. Garnet rim compositions have Mg#s of ranging from 77.8 to 82.5 and CaO contents of 3.8 to 5.6 wt%. TiO_2 and Cr_2O_3 contents are 0.5–1.0 wt% and 0.7 to 1.2 wt%, respectively.

Olivine. Mg#s of olivine varies from 90.0 to 90.6.

Magnesite. Magnesite is observed in iterations 1–3 and has Mg#s from 93.2 to 93.5 and CaO contents between 1.4 and 2.1 wt%.

Discussion

Approach to near-solidus melt composition using MISEs

Several criteria can be applied to assess whether iterative sandwich experiments produce melts characteristic of near-solidus partial melting of the target bulk composition. First, the iterations must converge such that the resulting melt and mineral compositions are comparable to those from preceding iterations. Second, the mineral compositions resulting from the experiments must match those present at the solidus of the target lithology at the temperature and pressure of the experiment.

In theory, if perfect equilibrium is achieved and if the estimates of the mineral/melt partition coefficients are similar to those prevailing at the solidus of the target bulk composition, the first MISE experiment should produce estimates of bulk partition coefficients $\left(\overline{D}_i s\right)$ and beginning at the second iteration, liquid and other phase compositions should be constant (Hirschmann and Dasgupta 2007). In the experiments presented here, some elements in some phases (e.g., SiO_2 in melt, FeO* in cpx) change little after the second iteration, but many other observed phase compositions vary noticeably through the first 3 iterations. Beginning at the third iteration, many elements in most phases reach concentrations that change little thereafter, and then virtually all elements in all phases change little in iterations 4 through 6 (Figs. 2, 3, 4, 5).

Calculated bulk partition coefficients, determined from the measured phase compositions of each experiment together with the phase proportions from the sub-solidus experiment with CO_2-free peridotite MixKLB-1 at 6.6 GPa and 1230°C (run M180; Table 2), fluctuate considerably between the first 3 iterations, but dampen noticeably thereafter (Fig. 6). Several factors may account for the delay in the number of iterations achieving steady state, including imperfect equilibration or differences in mineral/melt partition coefficients in the initial and later iterations. However, we believe that the principal factor that inhibited more rapid convergence was imperfections in initial estimates of $\overline{D}_i s$. These were likely exacerbated in the first iteration, where the analyzed surface of melt pools was damaged during sectioning with a wire saw.

Compositions of residual minerals in the iterative experiments also approach steady state after the fourth iteration (Figs. 3, 4, 5). Importantly, residual mineral compositions approach those found in the sub-solidus equilibration experiment (M180) for virtually every oxide. This provides strong evidence that the melt compositions observed in the later iterations are in equilibrium with the sub-solidus peridotite mineral compositions, meaning the melts are indicative of true near-solidus partial melts.

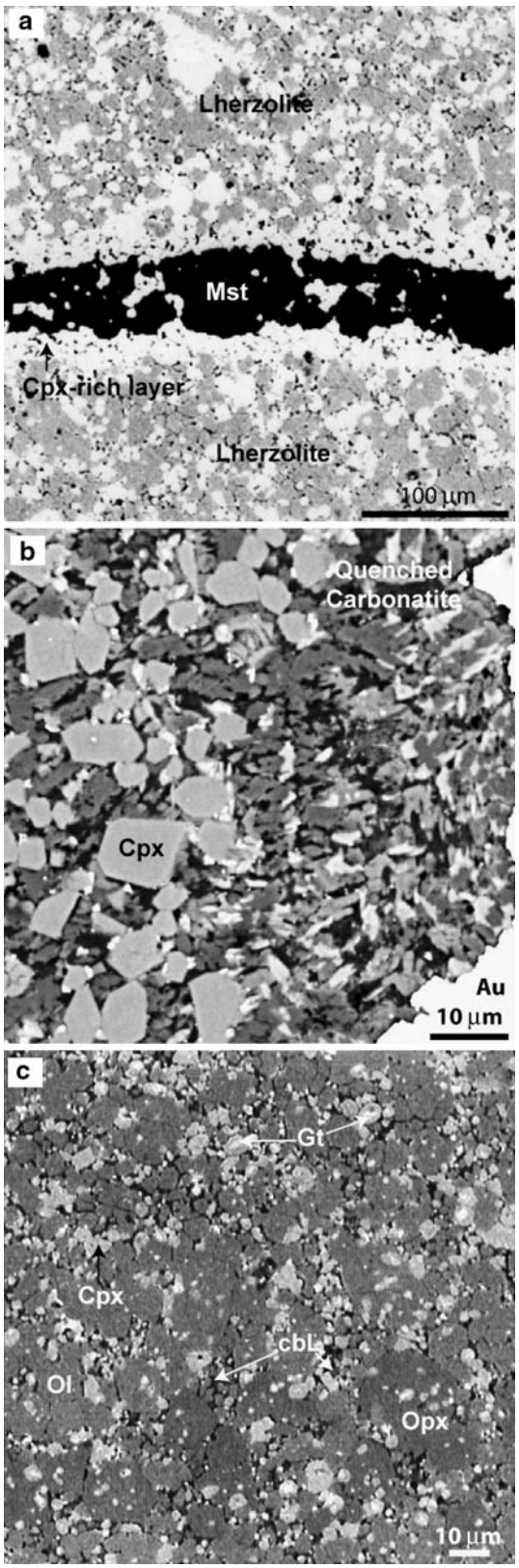

◀ **Fig. 1** Backscattered electron micrographs of quenched charges. **a** A layer of magnesite produced between peridotite layers at subsolidus conditions from a peridotite–carbonate sandwich in iteration# 3 (M277: 6.6 GPa, 1,200°C, 24 h). Cpx-rich skarns adjacent to the layer of magnesite indicate reaction between the CaO-rich introduced carbonate layer and the adjacent lherzolite. **b** A quenched pool of carbonatite located at one corner of the gold capsule in iteration# 2 (M265: 6.6 GPa, 1,230°C, 24 h) in presence of residual cpx. Back-scattered electron contrast and EDS analyses indicate that typical carbonatite melt pools quench to a complex assemblage comprising at least four different quench phases including an Mg-rich carbonate, a Ca–Mg carbonate, a sodium-rich carbonate, and cpx. **c** A portion of peridotite matrix 'bread' showing interstitial quenched carbonate melt at triple grain junctions and along grain edges of silicate minerals (M278: 6.6 GPa, 1,230°C, 24 h)

In a few cases, some oxide concentrations in some phases do not approach the composition of the sub-solidus minerals. One such exception is the Al_2O_3 concentration of opx, which was 1.42 ± 0.06 wt% in the sub-solidus experiment, but converges to 0.65 ± 0.02 wt% in iterations 4–6. This may be owing to failure to achieve equilibrium Al_2O_3 concentrations in the sub-solidus experiment. We note that the Al_2O_3 concentration in residual cpx from later iterations matches that of the sub-solidus experiment within analytical uncertainty. Thus, partitioning of Al_2O_3 between cpx and opx must not represent equilibrium in either the iterative experiments or the sub-solidus experiment. As an inter-granular melt promotes chemical exchange between mineral grains and as infiltration of carbonatitic melts is thought to incite dissolution-reprecipitation in mantle silicates (Hammouda and Laporte 2000), cpx/opx equilibrium is more probable in the melt-present experiments.

A second difference is that the olivine compositions in the iterative experiments converge to a Mg# 90.6, whereas the observed olivine in the sub-solidus experiment had a Mg# of 90.3. Also the garnet compositions converge to a Mg# of 81.8, whilst the subsolidus experiment has a Mg# of 77.8. These differences likely reflect a small amount of iron loss in the melt-present experiments. As indicated in Table 2, mass balance calculations are consistent with ~2% (relative) Fe loss during iterations 5 and 6. The difference in Mg#s between sub-solidus and the final melt-present olivines suggests about 3% (relative) Fe loss, which is within the uncertainty of the mass balance calculations.

Mean composition of near-solidus partial melt

Assuming that steady state was achieved beginning at the fourth iteration, the representative composition of solidus partial melt of peridotite + CO_2 at 6.6 GPa can be taken to be the mean of melt compositions from iterations four through six. Variations among these melt compositions can be taken to be representative of uncertainties stemming from analytical and procedural uncertainties of our method. The resulting composition (Table 3) has molar Ca/(Ca + Mg) of 0.413 ± 0.001 and Ca# [100 × molar Ca/

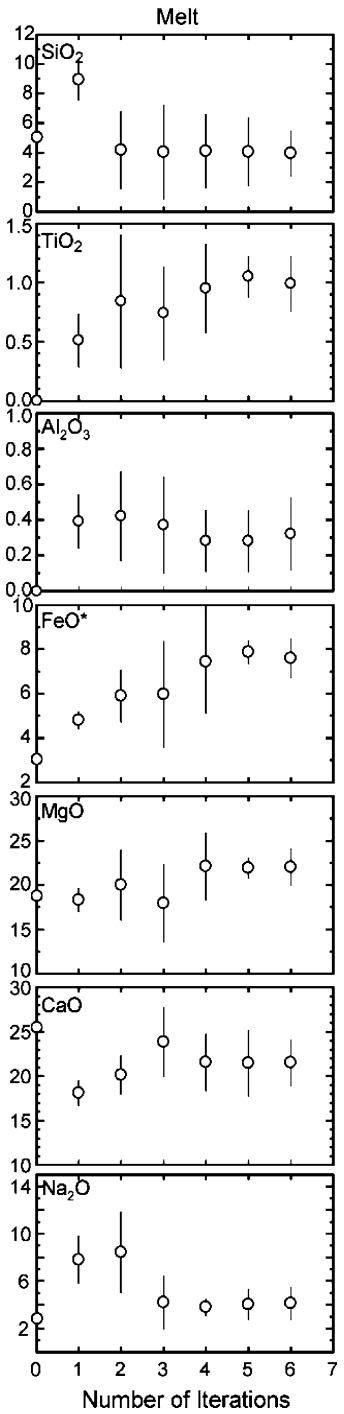

Fig. 2 Compositions of carbonatitic melt produced in modified iterative sandwich experiments at 6.6 GPa plotted versus the iteration number. Error bars are ± 1σ (wt%) based on replicate analyses. Based on the trend of oxide concentrations with the iteration, compositions from iterations 4 to 6 are taken to be representative of the near-solidus partial melt of carbonated peridotite. The composition plotted for the 0th iteration is that of the carbonate layer inserted into the first iteration

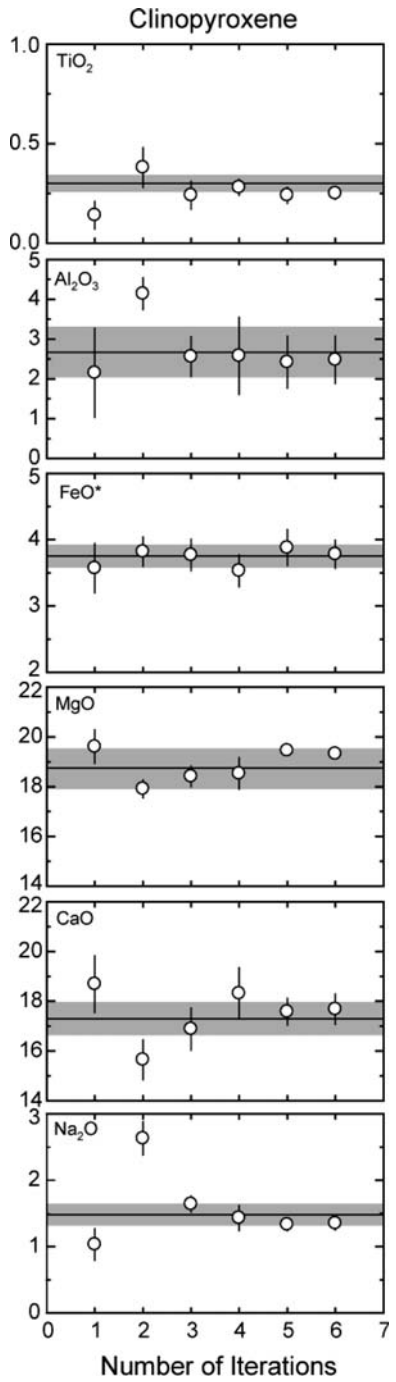

Fig. 3 Clinopyroxene compositions produced in modified iterative sandwich experiments at 6.6 GPa plotted versus the iteration number. Error bars are ± 1σ (wt%) based on replicate analyses. The *horizontal black line* and the *grey band* indicate the mean composition and ± 1σ uncertainty based on replicate analyses for cpx produced from the melt-free sub-solidus experiment with composition MixKLB-1 (M180: 6.6 GPa, 1,230°C, 48 h)

(Ca + Mg + Fe*)] of 37.1 ± 0.1. The mean SiO_2, concentration is 4.1 ± 0.1 and TiO_2 and Al_2O_3 concentrations are 1.0 ± 0.1, and 0.30 ± 0.02 wt%, respectively, whereas FeO* and Na_2O concentrations are 7.6 ± 0.2 and 4.0 ± 0.2 wt% respectively. The estimated CO_2 content, based on electron microprobe totals, is 39.2 ± 0.2 wt%.

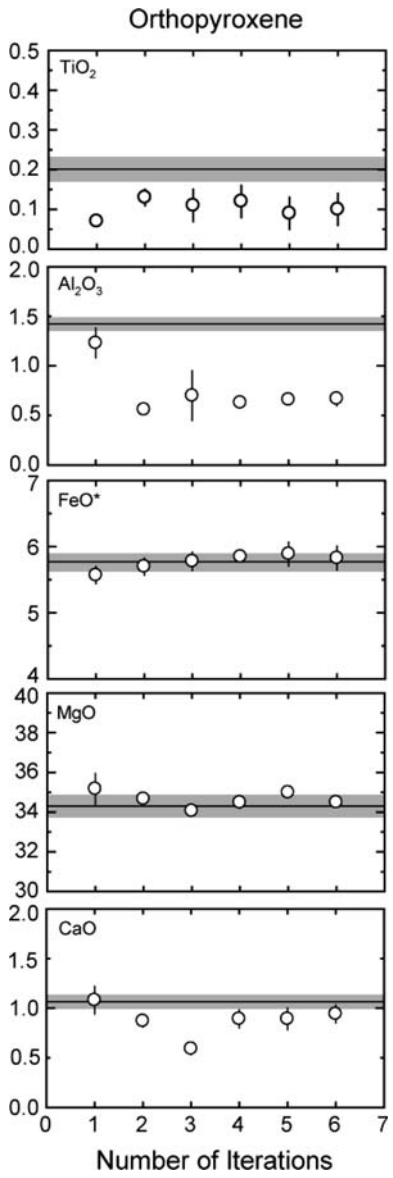

Fig. 4 Orthopyroxene compositions produced in modified iterative sandwich experiments. The other details are as in Fig. 3

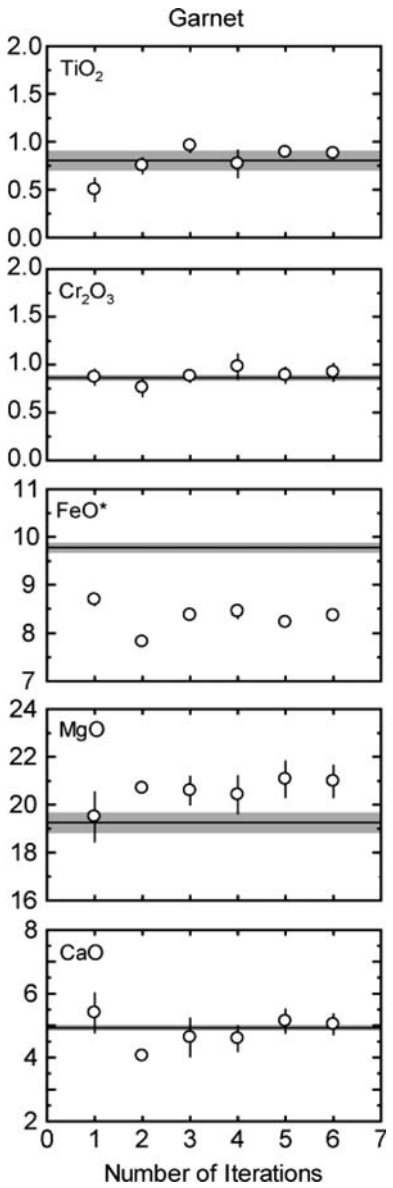

Fig. 5 Garnet compositions produced in modified iterative sandwich experiments. The other details are as in Fig. 3

Our estimate of the near-solidus carbonatite liquid composition does not include estimates of either K_2O or H_2O concentrations. Although we included some K_2O in the initial iteration, determination of low concentrations of K_2O in quenched melts and in residual minerals proved intractable with electron microprobe analysis. Other techniques, such as SIMS or LA-ICP-MS would be possibly more appropriate. The peridotite/carbonate partition coefficient for K_2O at 6.6 GPa is not well-constrained by experiment, but using the range of estimated by Dasgupta and Hirschmann (2006) $\left(\overline{D}_K = 0.004 - 0.1\right)$ and a depleted mantle composition of 0.006 wt% K_2O (Workman and Hart 2005), the near-solidus partial melt should have 0.6–1.5 wt% K_2O. Near-solidus partial melts of mantle slightly more enriched than true DMM depleted mantle could be accordingly more potassic. Similarly, our experiments were not well suited for measurment of H_2O either in the quenched carbonate melts or in the residual solids and the peridotite/carbonatite partition coefficient for H_2O is poorly known. Applying the value estimated by Dasgupta and Hirschmann (2006) $\left(\overline{D}_H = 0.004\right)$ and concentrations of H_2O in typical upper mantle of 50–200 ppm (Dixon et al. 1988; Michael 1988), the near-solidus carbonatite liquid could have between 1.25 and 5 wt% H_2O.

In all the analyzed carbonatite melts from iterations 4–6, the molecular proportion of network-modifying cations (K_2O, Na_2O, CaO, MgO, MnO, FeO*) exceeds that of

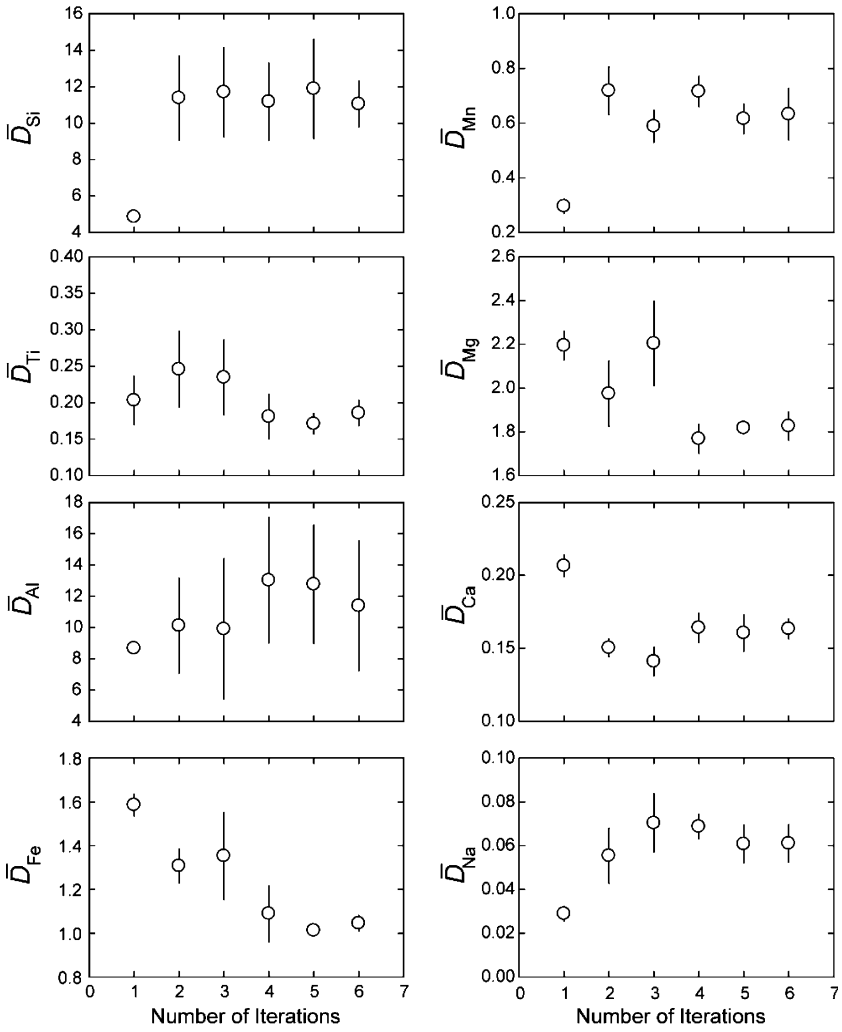

Fig. 6 Bulk partition coefficients $(\overline{D}_i s)$ for major and minor elements near the solidus of carbonated fertile peridotite at 6.6 GPa versus the iteration number. The $\overline{D}_i s$ were calculated from observed mineral/melt $\overline{D}_i s$ and the mode of minerals observed in experiment M180, as detailed in the text. Iterations 4 to 6 are thought to give estimates of $\overline{D}_i s$ that prevail near the solidus of natural carbonated peridotite at a depth of ~200 km

Table 9 Molecular composition of carbonatite partial melts

Run#	M282	M289	M295	Average
Iteration#	4	5	6	'Equilibrium' melt
$CaCO_3$	0.392	0.394	0.395	0.394
MCO_3*	0.460	0.452	0.452	0.455
Na_2CO_3	0.062	0.067	0.068	0.066
K_2CO_3	0.000	0.000	0.001	0.000
M_2SiO_4*	0.045	0.061	0.060	0.055
$MsiO_3$*	0.025	0.008	0.008	0.014
TiO_2	0.012	0.014	0.013	0.013
Al_2O_3	0.003	0.003	0.003	0.003
Cr_2O_3	0.001	0.001	0.001	0.001

* M = Mg, Fe, Mn

CO_2. This suggests that some of these cations are associated with network-forming species in the melt, of which the chief constituent is silica. To explore the significance of this cation excess, we construct a normative composition for the partial melt (Table 9), using the following procedure. We assume that all alkalis and Ca associate with carbonate. The remaining CO_2 is assumed to be associated with the other divalent cations M (= MgO, MnO, and FeO*). The left over divalent cations are assumed to be associated with silica, as a combination of orthosilicate (M_2SiO_4) and metasilicate ($MSiO_3$) species. Our assumption that all of the Ca and alkalis are associated with carbonate but that only some of the other divalent cations are bonded to CO_3^{2-} is guided by the greater propensity of Ca and alkalis to bond with CO_3^{2-} complexes in carbonated silicate glasses (Brooker et al. 2001). As shown in Table 9, this assumed speciation scheme suggests that orthosilicate species are more abundant in these melts than metasilicate species, which may be consistent with the relatively low silica activity required by the peridotite buffering assemblage at this pressure. This inference is predicated on the accuracy of the CO_2 concentrations determined from microprobe totals on rather complex materials and ignores possible complexation of network modifying cations with other highly charged ions (Ti^{4+}, Al^{3+}, Cr^{3+}). The key point,

however, is that the abundance of network modifying cations in these carbonatite exceeds that of the CO_3^{2-} ligand and that complexation of these network modifiers with silica and other highly charged cations likely has a significant influence on the activities of silicate and other species in carbonatitic melts.

Comparison of partial melt composition with previous partial melting studies of peridotite + CO_2

There are a range of previous experimental determinations of compositions of carbonatite partial melts in equilibrium with peridotitic mineral residua that are relevant to near-solidus partial melting of carbonated peridotite (Wallace and Green 1988; Thibault et al. 1992; Ryabchikov et al. 1989; Sweeny et al. 1994; Dalton and Presnall 1998; Moore and Wood 1998; Gudfinsson and Presnall 2005; Dasgupta and Hirschmann 2007). Among these studies, there are two types that are of greatest relevance to the compositions of partial melts anticipated at the onset of partial melting of carbonated peridotite: (1) multiple saturation experiments with simple system (CMAS) model carbonated peridotite (Dalton and Presnall 1998; Gudfinsson and Presnall 2005) and (2) iterative sandwich experiments defining the composition of near-solidus partial melt of carbonated peridotite at 2.2 and 3 GPa (Wallace and Green 1988; Thibault et al. 1992).

Dalton and Presnall (1998) determined the compositions of carbonated melt coexisting with ol + opx + cpx + gt + mst between 3 and 7 GPa through multiple saturation experiments in the system $CaO–MgO–Al_2O_3–SiO_2–CO_2$ (CMAS + CO_2). Because of the low variance of this synthetic system, melt compositions are isobarically invariant and therefore do not depend on melt fraction. However, the solidus temperature of CMAS + CO_2 peridotite at 6.6 GPa is ~150°C hotter than that observed for natural carbonated peridotite (Dasgupta and Hirschmann 2006). As other compositional differences between the two melts are rather subtle, this must be attributable chiefly to the solidus-lowering effect of the 7 wt% FeO* and 4 wt% Na_2O in the near-solidus liquids of the natural carbonated peridotite. One other notable difference is in the molar Ca/(Ca + Mg). As shown in Fig. 7, the molar Ca/(Ca + Mg) of the near-solidus liquid determined in this study plots significantly below the trend of molar Ca/(Ca + Mg) versus pressure for the CMAS + CO_2 liquids. The difference is likely attributable to the higher temperature solidi for the CMAS + CO_2 liquids, as the temperature dependence of Ca–Mg exchange between carbonate and cpx favours carbonate liquids with higher Ca/Mg at higher temperature (Dasgupta et al. 2005).

Wallace and Green (1988) and Thibault et al. (1992) performed conventional iterative sandwich experiments at 2.2 and 3 GPa, respectively, to determine the composition of carbonatitic melt at the solidus of carbonated peridotite. These studies differ in some respects from the present investigation because the melts were hydrous, as they were saturated in amphibole or phlogopite. Also, the phlogopite-saturated liquid of Thibault et al. (1992) contains 7 wt% K_2O. We also note that some caution is required in interpreting the results of Wallace and Green (1988) and Thibault et al. (1992), as they employed conventional iterative methodologies and just 3 or 5 iterative steps, respectively. Conventional iterative sandwich experiments may require many more iterations to converge, even for mildly incompatible elements such as Na (Hirschmann and Dasgupta 2007), and so it is possible that the reported liquid compositions do not represent true near-solidus partial melts.

Despite these differences, liquids from the studies of Wallace and Green (1988) and Thibault et al. (1992) are similar to those from the higher pressure results presented here in that they are all sodic iron bearing carbonatites with Ca/(Ca + Mg) similar to dolomite and with Mg#s close to 85. Among liquids in the three studies, the molar Ca/(Ca + Mg) ratio diminishes linearly with increasing pressure, a trend that parallels the trend observed for CMAS + CO_2 liquids by Dalton and Presnall (1998) (Fig. 7). Though more work at a range of pressures is needed, the trend defined by these data is the best available approximation of variation of Ca/(Ca + Mg) versus pressure along the solidus of natural carbonated peridotite. Finally, the liquids produced by Wallace and Green (1988) and Thibault et al. (1992) at 2.2–3 GPa have 5 wt% Na_2O, which is just slightly more than the 4 wt% found at 6.6 GPa in this study. The differences may possibly be attributable to a small pressure effect to pyroxene/melt partition coefficient of Na_2O.

Carbonatite–peridotite interaction in upwelling oceanic mantle

Carbonatitic partial melts produced at the solidus of carbonated peridotite will percolate upwards (Hunter and McKenzie 1989; Minarik and Watson 1995; Hammouda and LaPorte 2000). As they do so, their compositions will shift as they react with surrounding peridotite. Melts produced beneath ridges at ~300 km (Dasgupta and Hirschmann 2006) will remain carbonatitic until depths of ~120 km, at which point significant silicate dissolves in the melt, producing a carbonated silicate melt (Dasgupta et al. 2007). However, in the depth interval between ~300 and ~120 km, the composition of the carbonatite melt will shift owing to Ca–Mg–Fe–Na exchange with the peridotite. As illustrated in Fig. 7, with diminishing pressure, carbonatitic partial melts increase in Ca/(Ca + Mg) along the solidus.

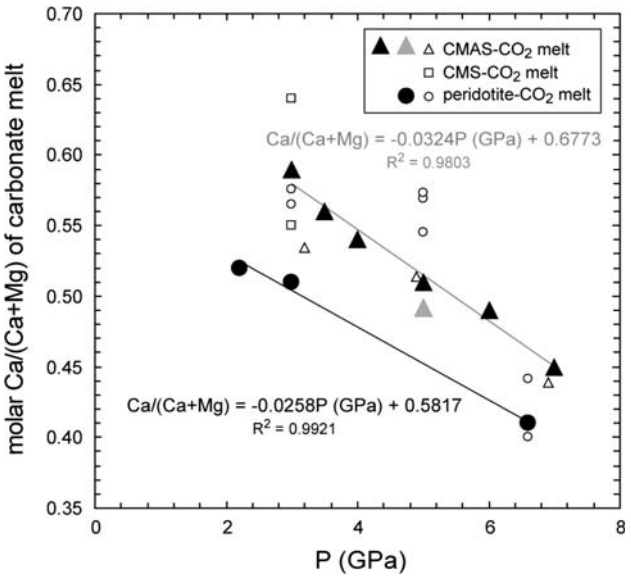

Fig. 7 Molar Ca/(Ca + Mg) of carbonatite melts relevant to near-solidus partial melting of carbonated peridotite, plotted as a function of pressure. Solid circles are for carbonatite partial melts stable near the solidus of peridotite, as determined from iterative sandwich experiments [natural peridotite + CO_2 at 2.2 GPa (Wallace and Green 1988), 3 GPa (Thibault et al. 1992), and 6.6 GPa (this study)]. *Black* (Dalton and Presnall 1998) and *grey* (Gudfinnsson and Presnall 2005) *triangles* are synthetic CMAS + CO_2 experiments in which liquids coexist with the isobarically invariant mineral assemblage (ol + opx + cpx + gt + mst) indicative of the synthetic peridotite solidus. *Open symbols* are carbonatite liquids from other peridotite + CO_2 phase equilibria studies [*triangles*: CMAS + CO_2 (Gudfinnsson and Presnall, 2005), *squares*: CMS + CO_2 (Moore and Wood 1998), *circles*: natural peridotite + CO_2 at 3 GPa (Dasgupta 2006), 5 GPa (Ryabchikov et al. 1989) and 6.6 GPa (Dasgupta and Hirschmann 2007)]. Partial melt compositions from calcite peridotite by Dalton and Wood (1993) at 1.5 to 3 GPa are significantly more calcic [molar Ca/(Ca + Mg) of 0.88 to 0.68] and are not included in this plot. The lines and equations give the compositions of primary carbonatitic partial melts stable near the solidus of carbonated peridotite (*black* natural peridotite + CO_2; *grey* CMAS + CO_2) as a function of pressure. Lower Ca/(Ca + Mg) for partial melts of natural peridotite compared to that of CMAS + CO_2 peridotite is owing to the lower solidus temperature of the latter (see text). The trend of decreasing Ca/(Ca + Mg) with pressure indicates that the incipient carbonatite partial melt extracted from upwelling peridotite at a depth of ~300–330 km (Dasgupta and Hirschmann 2006) would have a molar Ca/(Ca + Mg) of ~0.32

Partial melts percolating along an adiabat, rather than along the solidus, should show yet greater increases in Ca/(Ca + Mg), owing to the temperature dependence of carbonatite/silicate mineral equilibria (see previous section). Thus carbonatite melts reacting with surrounding peridotite will become progressively more calcic as they percolate upward through the convecting mantle, owing to reactions with pyroxenes such as

$$\underset{\text{melt}}{MgCO_3} + \underset{\text{cpx}}{CaMgSi_2O_6} \Rightarrow \underset{\text{melt}}{CaCO_3} + \underset{\text{opx}}{Mg_2Si_2O_6} \quad (1)$$

Dissolution of clinopyroxene owing to percolation of carbonatite melts through the convecting mantle contrasts with the effects of carbonatite percolation through the lithosphere, which is associated with a modal increase in clinopyroxene in lherzolite or complete conversion of lherzolite to wehrlite (Dalton and Wood 1993). Such reactions occur for one of three reasons. Carbonatite–peridotite interaction may be driven by low pressure decarbonation reactions such as

$$\underset{\text{opx}}{2Mg_2Si_2O_6} + \underset{\text{melt}}{CaMg(CO_3)_2} \Rightarrow \underset{\text{olivine}}{Mg_2SiO_4} + \underset{\text{cpx}}{CaMgSi_2O_6} + \underset{\text{vapor}}{CO_2} \quad (2)$$

(e.g., Canil 1990; Hauri et al. 1993; Yaxley et al. 1998). Alternatively, carbonatite–peridotite reactions occurring with decreasing temperature can produce increases in cpx owing to temperature-dependent Ca–Mg exchange between carbonatite melt and pyroxenes

$$\underset{\text{opx}}{Mg_2Si_2O_6} + \underset{\text{melt}}{CaMg(CO_3)_2} \Rightarrow \underset{\text{cpx}}{CaMgSi_2O_6} + \underset{\text{melt}}{2MgCO_3} \quad (3)$$

Finally, reactions between peridotite and calcic carbonatite melts generated from exotic lithologies such as carbonated eclogite (Dasgupta et al. 2004; Yaxley and Brey 2004) can also increase the mode of clinopyroxene in the lithosphere. This last reaction may also plausibly occur in the deep convecting mantle if carbonated eclogites are present (Dasgupta et al. 2006).

Conclusions

Iterative sandwich experiments equilibrating carbonate melt with peridotite residua at 6.6 GPa converge to the near-solidus partial melt composition after 4 iterations, thereby demonstrating the efficacy of the modified iterative sandwich experiment (MISE) method proposed by Hirschmann and Dasgupta (2007). The incipient melt derived at 200 km from peridotite with traces of sub-solidus carbonate is a sodic iron-bearing dolomitic carbonatite with molar Ca/(Ca + Mg) of 0.41, 4 wt% Na_2O and a Mg# of 84.

Acknowledgments We are thankful to an anonymous referee for constructive reviews. RD acknowledges support of the Graduate School of University of Minnesota through a Doctoral Dissertation Fellowship towards the early part of this study and Lamont-Doherty Earth Observatory of Columbia University for a post-doctoral research fellowship during preparation of the manuscript. The work also received support from NSF grants EAR 0310142 and EAR 0609967 to MMH.

References

Brooker RA, Kohn SC, Holloway JR, McMillan PF (2001) Structural controls on the solubility of CO_2 in silicate melts Part II: IR characteristics of carbonate groups in silicate glasses. Chem Geol 174:241–254

Canil D (1990) Experimental study bearing on the absence of carbonate in the mantle-derived xenoliths. Geology 18:1011–1013

Dalton JA, Presnall DC (1998) Carbonatitic melts along the solidus of model lherzolite in the system CaO-MgO-Al_2O_3–SiO_2–CO_2 from 3 to 7 GPa. Contrib Mineral Petrol 131:123–135

Dalton JA, Wood BJ (1993) The compositions of primary carbonate melt and their evolution through wallrock reaction in the mantle. Earth Planet Sci Lett 119:511–525

Dasgupta R (2006) Experimental investigation of mantle melting in the presence of carbonates. PhD Thesis. University of Minnesota, Minneapolis, p 247

Dasgupta R, Hirschmann MM (2006) Melting in the Earth's deep upper mantle caused by carbon dioxide. Nature 440:659–662

Dasgupta R, Hirschmann MM (2007) Effect of variable carbonate concentration on the solidus of mantle peridotite. Am Mineral 92:370–379

Dasgupta R, Hirschmann MM, Withers AC (2004) Deep global cycling of carbon constrained by the solidus of anhydrous, carbonated eclogite under upper mantle conditions. Earth Planet Sci Lett 227:73–85

Dasgupta R, Hirschmann MM, Dellas N (2005) The effect of bulk composition on the solidus of carbonated eclogite from partial melting experiments at 3 GPa. Contrib Mineral Petrol 149:288–305

Dasgupta R, Hirschmann MM, Smith ND (2007) Water follows carbon: CO_2 incites deep silicate melting and dehydration beneath mid-ocean ridges. Geology 35:135–138

Dixon JE, Stolper EM, Delaney JR (1988) Infrared spectroscopic measurements of CO_2 and H_2O in Juan de Fuca Ridge basaltic glasses. Earth Planet Sci Lett 90:87–104

Eggler DH (1976) Does CO_2 cause partial melting in the low-velocity layer of the mantle? Geology 4:69–72

Gudfinnsson G, Presnall DC (2005) Continuous gradations among primary carbonatitic, kimberlitic, melilititic, basaltic, picritic, and komatiitic melts in equilibrium with garnet lherzolite at 3–8 GPa. J Petrol 46:1645–1659

Hammouda T, Laporte D (2000) Ultrafast melt impregnation by carbonatite melts. Geology 28:283–285

Hauri EH, Shimizu N, Dieu JJ, Hart SR (1993) Evidence for hotspot-related carbonatite metasomatism in the oceanic upper mantle. Nature 365:221–227

Hirschmann MM, Dasgupta R (2007) A modified iterative sandwich method for determination of near-solidus partial melt compositions. I. Theoretical considerations. Contrib Mineral Petrol doi:10.1007/s00410-007-0213-9

Hunter RH, McKenzie D (1989) The equilibrium geometry of carbonate melts in rocks of mantle composition. Earth Planet Sci Lett 92:347–356

Marty B, Tolstikhin IN (1998) CO_2 fluxes from mid-ocean ridges, arcs and plumes. Chem Geol 145:233–248

Michael PJ (1988) The concentration, behavior and storage of H_2O in the suboceanic upper mantle: implications for mantle metasomatism. Geochim Cosmochim Acta 52:555–566

Minarik WG, Watson EB (1995) Interconnectivity of carbonate melt at low melt fraction. Earth Planet Sci Lett 133:423–437

Moore KR, Wood BJ (1998) The transition from carbonate to silicate melts in the CaO–MgO–SiO_2–CO_2 system. J Petrol 39(11 & 12):1943–1951

Pineau F, Shilobreeva S, Hekinian R, Bidiau D, Javoy M (2004) Deep-sea explosive activity on the Mid-Atlantic Ridge near 34°50′N: a stable isotope (C, H, O) study. Chem Geol 211:159–175

Ryabchikov ID, Brey G, Kogarko LN, Bulatov VK (1989) Partial melting of carbonatized peridotite at 50 kbar. Geokhimiya 1:3–9

Saal AE, Hauri E, Langmuir CH, Perfit MR (2002) Vapour undersaturation in primitive mid-ocean-ridge basalt and the volatile content of Earth's upper mantle. Nature 419:451–455

Sweeney RJ (1994) Carbonatite melt compositions in the Earth's mantle. Earth Planet Sci Lett 128:259–270

Thibault Y, Edgar AD, Lloyd FE (1992) Experimental investigation of melts from a carbonated phlogopite lherzolite: Implications for metasomatism in the continental lithospheric mantle. Am Mineral 77:784–794

Wallace ME, Green DH (1988) An experimental determination of primary carbonatite magma composition. Nature 335:343–346

Workman RK, Hart SR (2005) Major and trace element composition of the depleted MORB mantle (DMM). Earth Planet Sci Lett 231:53–72

Wyllie PJ, Huang W-L (1975) Influence of mantle CO_2 in the generation of carbonatites and kimberlites. Nature 257:297–299

Yaxley GM, Brey GP (2004) Phase relations of carbonate-bearing eclogite assemblages from 2.5 to 5.5 GPa: implications for petrogenesis of carbonatites. Contrib Mineral Petrol 146:606–619

Yaxley GM, Green DH, Kamenetsky V (1998) Carbonatite metasomatism in the southern Australian lithosphere. J Petrol 39:1917–1930